J Nanopart Res (2013) 15:1380
DOI 10.1007/s11051-012-1380-9

RESEARCH PAPER

Template synthesis of braided gold nanowires with gemini surfactant–$HAuCl_4$ aggregates

Wentao Wang · Yuchun Han · Mingyuan Gao · Yilin Wang

Received: 30 September 2012 / Accepted: 14 December 2012

Abstract One-dimensional braided gold nanowires with 40–50 nm in width and several micrometers in length which were fabricated by using cationic gemini surfactant hexamethylene-1,6-bis (dodecyl dimethylammonium bromide) ($C_{12}C_6C_{12}Br_2$). Through simply regulating the mole ratio of $C_{12}C_6C_{12}Br_2$ to $HAuCl_4$, the morphology of the gold products changed into nanoparticles and nanowires. The CryoTEM images indicated that the $C_{12}C_6C_{12}Br_2/HAuCl_4$ mixture formed spherical or fibrillar aggregates depending on the mole ratio of $C_{12}C_6C_{12}Br_2$ to $HAuCl_4$, which performed as the versatile templates for morphology-controlled synthesis of the multiple gold nanomaterials. The HRTEM and SAED results suggested the nanowires and braided nanowires were polycrystalline. The gold nanostructure displayed a time-dependent growth process, i.e., first the nanoparticles arranged in one dimension, and then assembled into nanowires. Therefore, a template-directed aggregation and fusion process of nanoparticles is proposed for the formation of the one-dimensional gold nanomaterials. The braided nanowires exhibited a higher catalytic activity in the reduction of *p*-nitroaniline than that of the nanowires. This gemini surfactant-based template provides a versatile strategy for the morphology-controlled synthesis of gold nanomaterials, and may be applied for the synthesis of other noble-metal nanomaterials.

Keywords Braided gold nanowire · Gemini surfactant · $C_{12}C_6C_{12}Br_2$–$HAuCl_4$ aggregates · Template

Introduction

Gold nanomaterials with tailored morphologies have received intense attention due to their fascinating morphology-dependent optical, electronic, and catalytic properties, etc. (Daniel and Astruc 2004; Cobley et al. 2011). During the past decades, great success has been achieved in the fabrication of gold nanomaterials with different morphologies, such as rods (Nikoobakht and El-Sayed 2003), wires (Kim et al. 2008), belts (Zhang et al. 2006), tubes (Banerjee et al. 2003), cages (Skrabalak et al. 2008), cubes (Habas et al. 2007), polyhedrons (Jeong et al. 2009), plates (Millstone et al. 2009), stars (Sau and Murphy 2004), multipods (Chen et al. 2007a), and so on. Among these nanomaterials, one-dimensional (1D) gold nanomaterials are

---

Electronic supplementary material The online version of this article (doi:10.1007/s11051-012-1380-9) contains supplementary material, which is available to authorized users.

W. Wang · Y. Han · M. Gao (✉) · Y. Wang (✉)
Key Laboratory of Colloid and Interface Science, Beijing National Laboratory for Molecular Sciences (BNLMS), Institute of Chemistry, Chinese Academy of Sciences, Beijing 100190, People's Republic of China
e-mail: gaomy@iccas.ac.cn

Y. Wang
e-mail: yilinwang@iccas.ac.cn

especially important because of potential applications in the fields of optics, electronics, chemical, and biosensing, nanomedicines (Chen et al. 2007b; Huang et al. 2009; Pérez-Juste et al. 2005; Sharma et al. 2009). Various methods such as lithography (Vazquez-Mena et al. 2008), seed-mediated growth (Nikoobakht and El-Sayed 2003; Murphy et al. 2011), and template synthesis (Xiao and Qi 2011; Kijima et al. 2004) have been used to fabricate 1D gold nanomaterials. However, to date, a majority of the reported 1D gold nanomaterials were of individual nanorod, nanowire or nanobelt. The hierarchical 1D gold nanowire composed of several individual nanowires has long been a missing piece of gold nanomaterials. Very recently, Wang and coworkers (2011) demonstrated an example to construct the alloy nanowires with well-defined double helical features. Upon growth of a thin metal (Pd, Pt or Au) layer on a chiral Au–Ag alloy nanowire, the nanowire winded around preformed Au–Ag nanowire to give a metallic double helix. It is highly desirable to search other feasible approaches to manipulate individual gold nanowires into hierarchical 1D nanowires.

Template-directed synthesis is a simple way to control the morphology of inorganic nanomaterials (Pileni 2003). Surfactant can self-assemble into various well-defined nanostructures, such as spherical and worm-like micelles, vesicles, and lamellar structures, which have been used to template synthesis of inorganic nanomaterials (Holmberg 2004). Although various surfactants have been applied to form ordered aggregates in aqueous solution to be templates for the synthesis of various nanomaterials (Lin and Mou 2002; Wan and Zhao 2007; Jana 2005), the template mechanism for gold nanomaterials has not been well-established. In general, surfactant aggregates are a class of dynamic molecular assemblies and may lose its structure in the presence of inorganic precursor or reducing agent (Qiao et al. 2011). Therefore, how to control the surfactant aggregate structures into the final resultant nanomaterials is a key step. More recently, a few studies illustrated that surfactant–metal complexes (Lu et al. 2008; Li et al. 2010; Han et al. 2008; Yi and Gao 2011) or metal-driven surfactant supermolecules (Qiao et al. 2011) are relatively stable and can be used as reactive templates. The resultant nanomaterials keep the morphology of template counterparts. Xiao and Qi (2011) have commendably reviewed the recent progress in the gold nanomaterial synthesis assisted by single/mixed surfactants and surfactant-metal complex templates.

Importantly, some novel surfactant aggregates can be realized by varying surfactant molecular structures and the solution conditions (Fan et al. 2011; Wu et al. 2010; Hou et al. 2010; Deng et al. 2009). Accordingly, novel nanostructures could be constructed through changing surfactant structures as well as their surroundings. Gemini surfactants are constructed by two hydrophobic chains and two polar/ionic headgroups covalently connected by a spacer group at the headgroup level (Menger and Keiper 2000). Due to their special self-assembly ability, they are superior to the corresponding conventional single-chain surfactants, such as remarkably low critical micellar concentration (CMC), high surface activity, unusual rheological properties, various aggregate structures, strong adsorptive ability, and so on (Han and Wang 2011). Owing to these unique properties, gemini surfactants have been considered as a kind of excellent candidates to replace conventional single-chain surfactants in template synthesis of gold nanofibers (Esumi et al. 1998) and nanoribbons (Bakshi et al. 2008). Furthermore, due to the high surface charge density of the aggregates constructed by ionic gemini surfactants, the aggregate transitions are highly sensitive to inorganic precursors. In the synthesis of gold nanomaterials, surfactant-precursor complexes (Li et al. 2010) can be formed spontaneously, which greatly influences the aggregation behavior of surfactants. To reveal intrinsic formation mechanism of the gold nanoparticles, it is essential to investigate the nature of the mixed systems of inorganic precursors with surfactants before nanomaterial reduction. It was found that a small amount of Cu^{2+} ions transform the micelles of anionic carboxylate gemini surfactant SDUC into vesicles due to the formation of Cu^{2+}-SDUC complexes, and Cu^{2+} can induce the fusion/fission of the vesicles with time (Huang et al. 2006). Therefore, modulating the interaction between gemini surfactants and ionic precursors may generate mixed aggregates with special structures and the aggregates may be applied as templates for constructing nanomaterials.

Herein, novel hierarchical 1D gold nanowires, braided nanowires, are successfully constructed using gemini surfactant–$HAuCl_4$ aggregates as the templates. To better understand the mechanism, systematic studies were performed to illustrate the aggregate transitions of $C_{12}C_6C_{12}Br_2$ upon the addition of $HAuCl_4$. The formation mechanism of the gold nanomaterials has been proposed. Furthermore, the catalytic activity of the as-prepared braided nanowires was investigated.

Experimental section

Materials

Chloroauric acid ($HAuCl_4 \cdot 4H_2O$, 99.9 %,) was purchased from Shenyang Jinke Reagents Company. Sodium borohydride ($NaBH_4$) and *p*-nitroaniline (*p*-NA) of analytical grade were obtained from Beijing Chemical Reagents Plant. Gemini surfactant hexamethylene-1,6-bis (dodecyl dimethylammonium bromide) ($C_{12}C_6C_{12}Br_2$) was synthesized as reported in the literature (Zana et al. 1991) and was used after repeated recrystallization from ethanol. Ultrapure water (Milli-Q, 18.2 MΩ cm) was used to prepare all the solutions.

Preparation of gold nanomaterials

As a typical procedure, 200 μL of $C_{12}C_6C_{12}Br_2$ solution (100 mM) was injected into 9 mL of water and vortexed. After 30 min, 641 μL of $HAuCl_4$ aqueous solution (15.6 mM) was added into this surfactant aqueous solution and mixed, then the mixture solution was held at 25 °C for 12 h. After 12 h aging, the 150 μL of ice-cold freshly prepared $NaBH_4$ (400 mM) was rapidly injected into the above mixture with vigorously stirring for 1 min, and then the reaction mixture was kept at 25 °C under static condition for 24 h. The solution was centrifuged at 2,000 rpm for 20 min. Then the supernatant was removed and ultrapure water was added to the precipitate. The residue was dispersed by sonication for 3 min. The rinsing procedure was repeated at least three times to obtain the final gold nanomaterials.

Characterization of $C_{12}C_6C_{12}Br_2$–$HAuCl_4$ aggregates

All the $C_{12}C_6C_{12}Br_2$–$HAuCl_4$ solutions used in preparation of gold nanomaterials underwent an aging time of 12 h. After 12 h, suspensions appeared in solutions with the $C_{12}C_6C_{12}Br_2$/$HAuCl_4$ mol ratio (*R*) of 10:1, 2:1, 1:1, and 1:2, while the solutions were kept transparent at the *R* of 50:1 and 20:1. The $C_{12}C_6C_{12}Br_2$–$HAuCl_4$ solutions were characterized by UV–Vis spectroscopy (Shimadzu, UV-1601), X-ray diffraction (XRD, Rigaku D/max-2500, Cu Kα radiation, 40 kV, 200 mA) and Cryogenic Transmission Electron Microscopy (CryoTEM, FEI Tecnai 20, 200 kV). The UV–Vis absorption spectra of the precursor solution were recorded from 190 to 700 nm using a quartz cell with 0.5 cm path length. For the XRD sample preparation, the suspension was centrifuged at 5,000 rpm for 10 min. The supernatant was drawn off with a syringe and the yellow solid was dried by freeze-dry and vacuum-dry in sequence. The XRD patterns of the samples were recorded in the range of 2–6° with a scanning speed of 1.2°/min. For the CryoTEM grid preparation, 3.5 μL of precursor solutions were embedded in thin layer of vitreous ice on freshly carbon-coated holey TEM grids by blotting the grids with filter paper (blotting time was 3.5 or 4 s) and then plunging into liquid ethane cooled by liquid nitrogen. Frozen hydrated specimens were imaged by using the low-dose mode (about 2,000 e/nm^2) at about −174 °C.

Characterization of gold nanomaterials

The synthetic gold nanomaterials were characterized by transmission electron microscopy (TEM, FEI Tecnai spirit, 120 kV), high-resolution TEM, selected area electron diffraction (HRTEM and SAED, JEM-2011, 200 kV), and XRD. TEM grids were prepared by placing one drop of the aqueous dispersion of gold product on carbon-coated copper grids, allowing water to evaporate at ambient temperature. For the XRD measurements, several drops of gold product aqueous dispersion were dropped on a glass slide, followed by drying naturally in the air.

Catalytic activities of gold nanomaterials

The reduction of *p*-NA by $NaBH_4$ using the as-prepared gold nanomaterials as catalysts was conducted in aqueous solution. Gold nanowires, braided gold nanowires, and broad braided gold nanowires were used to investigate the catalytic properties. As the typical procedure, 0.3 mL of *p*-NA stock solution (1.0 mM) was mixed with 2.4 mL of water in the quartz cell and stirred for homogenization. Consecutively, 0.02 mL aqueous dispersion of gold nanowires

(1 mg/1 mL) was added to the above *p*-NA aqueous solution. Finally, 0.3 mL of ice-cold freshly prepared $NaBH_4$ aqueous solution (100 mM) was added to the reaction mixture. The reduction of *p*-NA was monitored with a spectrophotometer in the range 200–700 nm at ambient temperature.

Results and discussion

Synthesis of gold braided nanowires with gemini surfactant $C_{12}C_6C_{12}Br_2$

A special kind of gold nanostructure-like braided nanowires was obtained in the presence of the cationic gemini surfactant $C_{12}C_6C_{12}Br_2$. Figure 1a shows the typical braided nanowires with 40–50 nm in width and several micrometers in length synthesized by adding $NaBH_4$ to a solution of 0.2 mM $C_{12}C_6C_{12}Br_2$ and 0.2 mM $HAuCl_4$. The high-magnification TEM image of the braided nanowires shown in Fig. 1b clearly illustrates that the structure is composed of several nanowires interlaced together. To obtain the crystallographic structure information, SAED, HRTEM, and XRD measurements were employed. The SAED pattern (the inset of Fig. 1b) shows apparent diffractive rings that can be indexed as the gold polycrystalline face-centered-cubic (fcc) form. Figure 1c is the HRTEM image of a tiny part of the braided nanowires. Two types of lattice planes with the *d* spaces of 0.23 and 0.20 nm exist in the image, which can be ascribed to the (111) and (200) lattice spaces. The lattice fringes in different regions possess different orientations, indicating the braided nanowires are composed of small nanoparticles arranged in different directions. Besides, the XRD pattern of the braided nanowires (Fig. 1d) exhibits five sharp diffraction peaks exclusively ascribed to gold crystals with a fcc structure (JCPDS No. 04-0784), indicating that the braided nanowires are pure gold crystals.

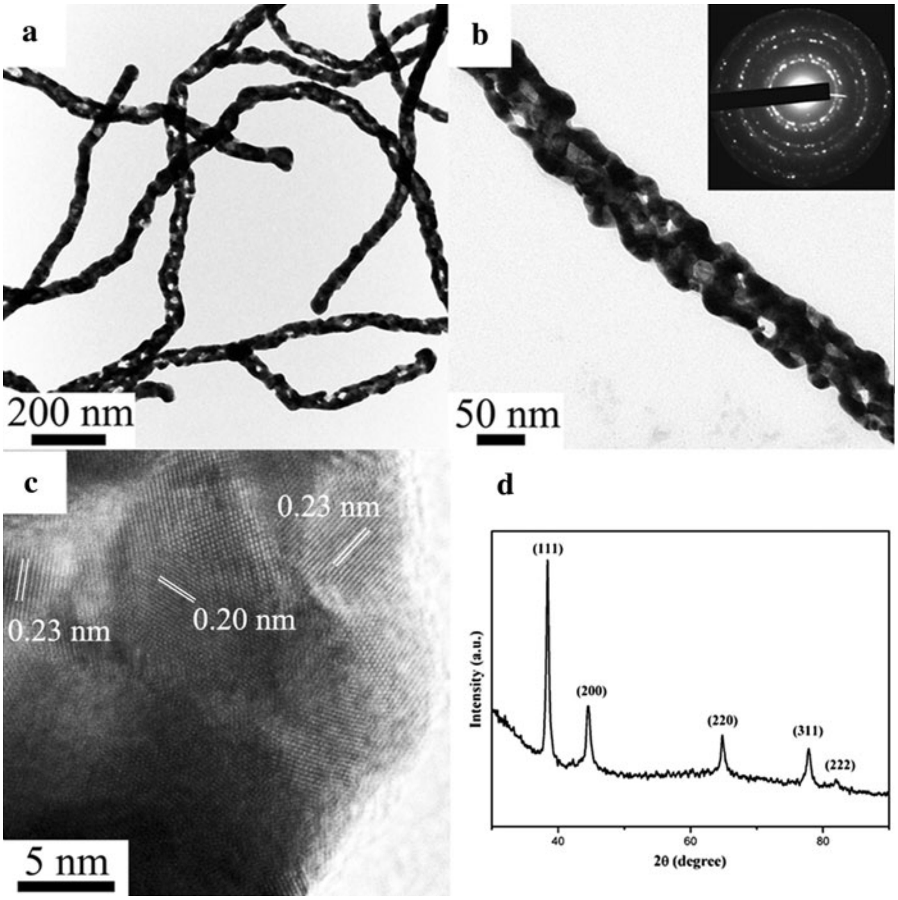

Fig. 1 TEM (**a**, **b**), HRTEM (**c**) images and XRD pattern (**d**) of the braided nanowires from reduction of 0.2 mM $HAuCl_4$ in the presence of 0.2 mM $C_{12}C_6C_{12}Br_2$. *Insets* show the related SAED pattern. $[NaBH_4]/[HAuCl_4] = 6$

Effects of $C_{12}C_6C_{12}Br_2/HAuCl_4$ molar ratio R on gold nanostructures

To better understand the formation mechanism of the braided nanowires, the relationship between the product morphologies and experimental conditions has been investigated. Fixing the $HAuCl_4$ concentration at 0.2 mM, the effect of R on the morphologies of gold products was studied. As illustrated in Fig. 2, a remarkable morphology evolution of nanoparticles → nanowires → braided nanowires → broad braided nanowires is observed with the decrease of the R. At $R = 50{:}1$ and 20:1, the gold products are spherical nanoparticles with an average diameter of ~10 nm (Fig. 2a) and ~15 nm (Fig. 2b), respectively. When R decreases to 10:1, the products transform into nanowires with hundreds of nanometers in length and ~20 nm in diameter, which coexist with a small quantity of short nanorods and nanoparticles (Fig. 2c). With further decreasing R to 2:1, the gold nanowires become 20–30 nm in diameter and several micrometers in length (Fig. 2d). Especially at $R = 1{:}1$, the braided nanowires are generated (Fig. 1a). At $R = 1{:}2$, the braided nanowires grow broadly with 100–120 nm in width and about 1 μm in length (Fig. 2e, f).

The SAED, HRTEM, and XRD measurements were also investigated for the nanowires and broad braided nanowires (Fig. S1). Both the SAED and HRTEM results suggest the obtained products are polymorphism. Several groups of inconsecutive lattice planes with the d space of 0.23 or 0.2 nm correspond to the (111) or (200) lattice space of fcc gold. This indicates that the nanowires and broad braided nanowires are also constructed of small nanoparticles. The XRD patterns of these two gold nanomaterials show a typical fcc gold diffraction pattern with five major peaks, corresponding to the (111), (200), (220), (311), and (222) reflection planes, respectively.

Aggregate structures in the $C_{12}C_6C_{12}Br_2$–$HAuCl_4$ precursor solution

In order to understand the mechanism of the formation of the gold nanomaterials above, the $C_{12}C_6C_{12}Br_2$–$HAuCl_4$ precursor solutions were investigated before reduction. Figure 3 shows the UV–Vis spectra of the $C_{12}C_6C_{12}Br_2$ aqueous solution, the $HAuCl_4$ aqueous solution and the mixed $C_{12}C_6C_{12}Br_2/HAuCl_4$ solution at different R. The UV–Vis absorption spectrum of the $C_{12}C_6C_{12}Br_2$ aqueous solution (a) shows an intense absorption at 200 nm due to bromide ions. The spectrum of the $HAuCl_4$ aqueous solution (b) presents two absorption peaks around 220 and 296 nm, which are ascribed to the charge transfer and *d–d* transition bands (Esumi et al. 1998). For the $C_{12}C_6C_{12}Br_2/HAuCl_4$ mixture at $R = 2{:}1$ (c), the charge transfer band undergoes a significant red-shift to 272 nm, and the *d–d* transition band splits into double peaks at around 415 and 486 nm. Then, the charge transfer and *d–d* transition bands shift to 256 and 356 nm for $R = 1{:}1$ (d) and 244 and 342 nm for $R = 1{:}2$ (e). In the $C_{12}C_6C_{12}Br_2$–$HAuCl_4$ mixtures at $R = 2{:}1$, 1:1, and 1:2, each $AuCl_4^-$ anion nearly binds with four, two or one quaternary ammonium ions of the $C_{12}C_6C_{12}Br_2$ molecules. These band shifts are attributed to the formation of the $C_{12}C_6C_{12}Br_2$–$HAuCl_4$ complexes by strong electrostatic interaction of the quaternary ammonium headgroups of $C_{12}C_6C_{12}Br_2$ with the $AuCl_4^-$ anions.

Figure 4 presents the representative CryoTEM images of the $C_{12}C_6C_{12}Br_2$–$HAuCl_4$ aggregates. With decreasing R, the aggregate morphologies of the $C_{12}C_6C_{12}Br_2$–$HAuCl_4$ complexes evolve from spherical aggregates of 20–40 nm in diameter at $R = 50{:}1$ to well-defined nanofibers with length in micrometers and 30–50 nm in diameter at $R = 2{:}1$. Continuously, the diameter of the fibers increases to 70–90 nm at $R = 1{:}1$, and 120–180 nm at $R = 1{:}2$.

At $R = 50{:}1$, the $C_{12}C_6C_{12}Br_2$–$HAuCl_4$ mixture forms spherical complex aggregates (Fig. 4a) rather than normal small micelles, because the $AuCl_4^-$ anions bind with $C_{12}C_6C_{12}Br_2$ through strong electrostatic interaction and in turn reduces the electrostatic repulsion between the head groups of the $C_{12}C_6C_{12}Br_2$ molecules. With decreasing R to 2:1, the electrostatic repulsion between the headgroups of $C_{12}C_6C_{12}Br_2$ is further weakened by the binding of the $AuCl_4^-$ anions, which leads to the increase of the packing parameter of the surfactant. Since the XRD spectrum of the fibrils (Fig. 5a) does not show a layer structure, the observed $C_{12}C_6C_{12}Br_2$–$HAuCl_4$ fibrils (Fig. 4b) should be formed by worm-like aggregates. Further decreasing R to 1:1 and 1:2, the significant reduction of electrostatic repulsion between the $C_{12}C_6C_{12}Br_2$ headgroups broadens the $C_{12}C_6C_{12}Br_2$–$HAuCl_4$ fibrils (Fig. 4c, d). According to the related XRD data (Fig. 5b, c), the diffraction peaks around $2\theta = 2.7°$ indicate the existence of layer structure with the d space of about 3.2 nm. The calculated length of a completely

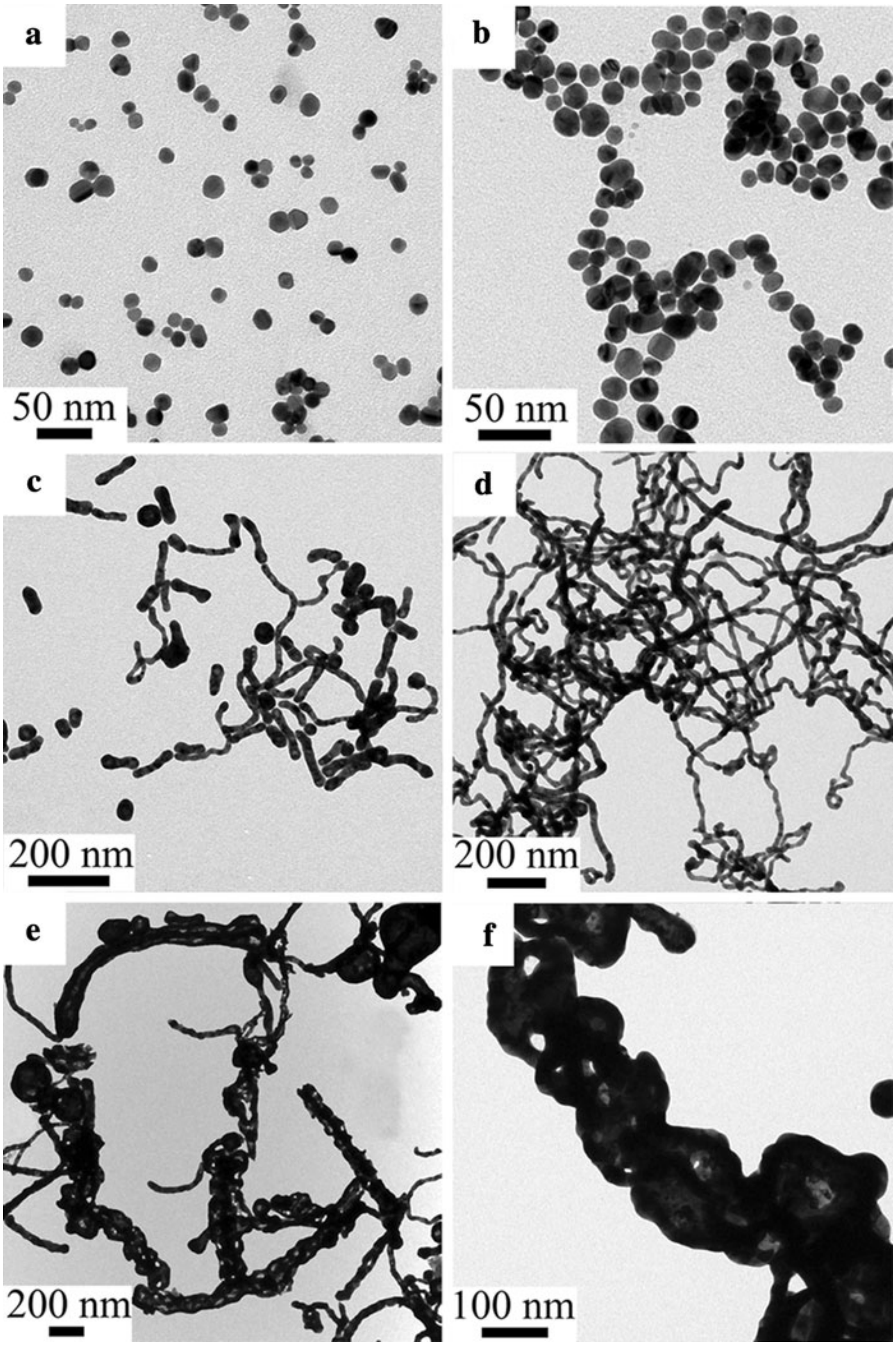

Fig. 2 TEM images of the gold nanomaterials from reduction of 0.2 mM $HAuCl_4$ with different R of 50:1 (**a**), 20:1 (**b**), 10:1 (**c**), 2:1 (**d**) and 1:2 (**e** and **f**). $[NaBH_4]/[HAuCl_4] = 6$

extended cationic alkyl chain of $C_{12}C_6C_{12}Br_2$ is around 1.7 nm. Therefore, double layer structures exist in the $C_{12}C_6C_{12}Br_2$–$HAuCl_4$ fibrils. That is to say, the $C_{12}C_6C_{12}Br_2/HAuCl_4$ mixtures form $C_{12}C_6C_{12}Br_2$–$HAuCl_4$ complexes are at different R and then form aggregates with different morphologies.

On the basis of the above results, the corresponding relationship of the aggregates of the $C_{12}C_6C_{12}Br_2$–$HAuCl_4$ complexes with the reduced gold

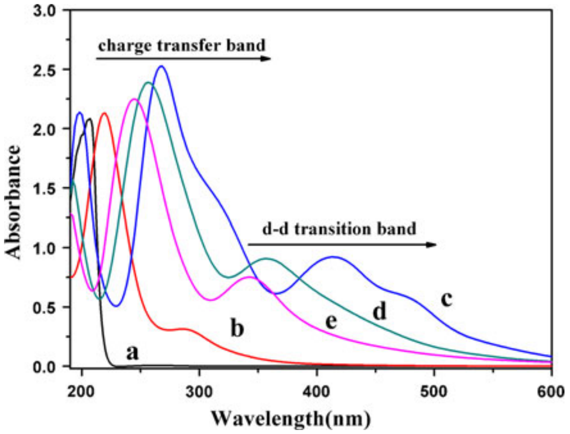

Fig. 3 UV–Vis spectra of 0.4 mM $C_{12}C_6C_{12}Br_2$ (*a*), 0.2 mM $HAuCl_4$ aqueous solution (*b*), the mixture solutions of 0.4 mM $C_{12}C_6C_{12}Br_2$ and 0.2 mM $HAuCl_4$ (*c*), 0.2 mM $C_{12}C_6C_{12}Br_2$ and 0.2 mM $HAuCl_4$ (*d*), and 0.1 mM $C_{12}C_6C_{12}Br_2$ and 0.2 mM $HAuCl_4$ (*e*)

nanomaterials is summarized as follows: the $C_{12}C_6C_{12}Br_2$–$HAuCl_4$ spherical aggregates at $R = 50{:}1$ yield gold nanoparticles, while the $C_{12}C_6C_{12}Br_2$–$HAuCl_4$ nanofibrils with various diameters yield nanowires at $R = 2{:}1$, braided nanowires at $R = 1{:}1$, and broad braided nanowires at $R = 1{:}2$. Obviously, the morphologies of the gold nanomaterials closely correlate with the morphologies of the $C_{12}C_6C_{12}Br_2$–$HAuCl_4$ aggregates. Accordingly, the $C_{12}C_6C_{12}Br_2$–$HAuCl_4$ aggregates are served as the templates for the formation of the gold nanomaterials.

Mechanism of morphological evolution of gold nanomaterials

Based on the above investigation and discussion, the possible mechanism of the morphology evolution of the gold nanomaterials is proposed as follows.

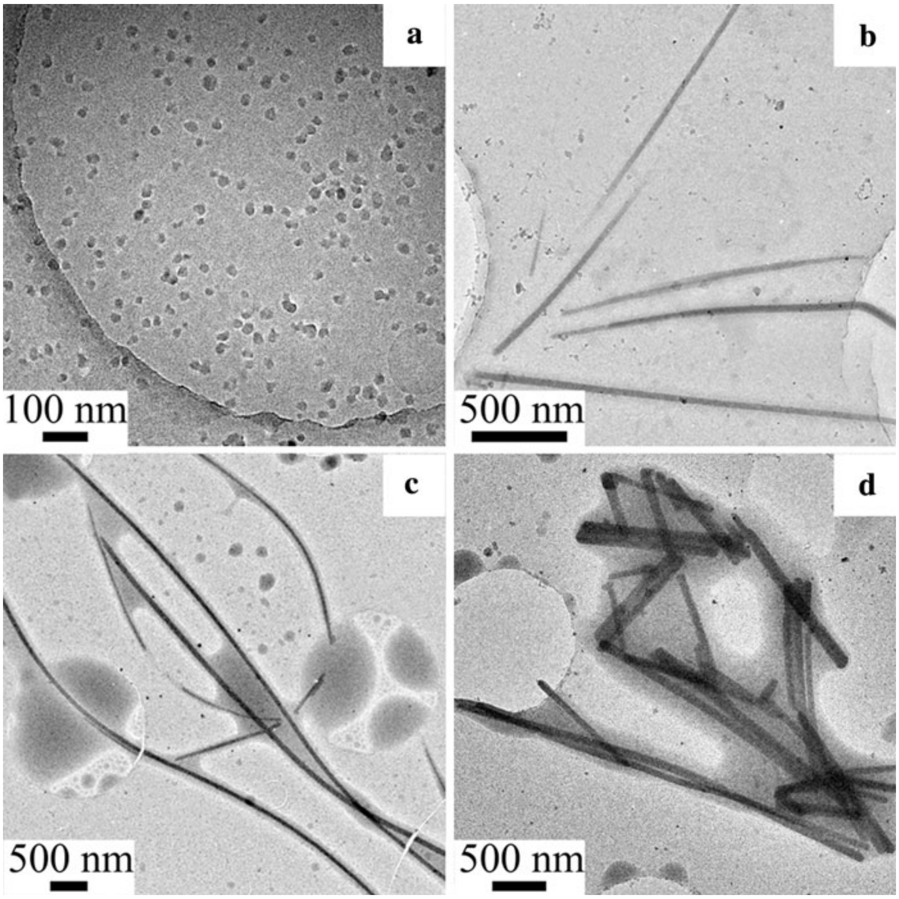

Fig. 4 CryoTEM images of the $C_{12}C_6C_{12}Br_2$–$HAuCl_4$ aggregates after 12 h aging. $R = 50{:}1$ (**a**), 2:1 (**b**), 1:1 (**c**), and 1:2 (**d**)

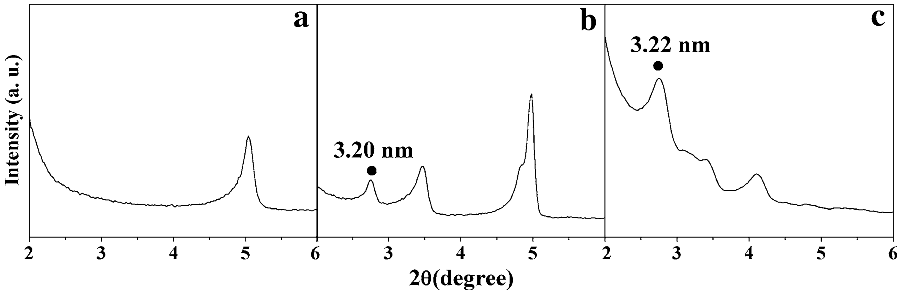

Fig. 5 XRD patterns of the $C_{12}C_6C_{12}Br_2$–$HAuCl_4$ aggregates at $R = 2:1$ (**a**), 1:1 (**b**), and 1:2 (**c**). $[HAuCl_4] = 0.2$ mM

Although, the micelle template mechanism is well-established in the synthesis of mesoporous materials, the template mechanism in the synthesis of metal nanoparticles is illusive (Xiao and Qi 2011; Qiao et al. 2011). It is commonly considered that surfactant molecules act as capping agents or particle stabilizers in the synthesis of metal nanoparticles. Up to now, the available templates for colloidal synthesis of gold nanocrystals are still limited. Jana (2005) demonstrated that CTAB cylindrical micelles could perform as templates at the early stage of gold nanorods growth. If the seed size was smaller than 3 nm and the growth rate were properly controlled, the growing nanoparticles (seed) absorbed on the micelle surface and grew along the long axis direction of the micelles. But if the seed size was larger than 3 nm, the nanoparticles were detached from the micelles due to the larger mass, and the micelles could not work well as templates. Normally micelles are in a dynamic equilibrium with monomers. Monomer-micelle exchange takes place in microseconds (Groth et al. 2004). Consequently, micelles are not stable enough to preserve the shape during the complex nucleation and growth of metal nanoparticles. However, compared with conventional surfactants, gemini surfactants have much slower monomer-micelle exchange kinetics (Ulbricht and Zana 2001). Moreover, the electrostatic repulsion between the headgroups of $C_{12}C_6C_{12}Br_2$ is greatly weakened through binding with the $AuCl_4^-$ anions in the $C_{12}C_6C_{12}Br_2$–$HAuCl_4$ aggregates, which leads to the formation of compact structures in the aggregates and further reduces the monomer-micelle exchange. In addition, the gemini surfactant has much stronger hydrophobic interaction and the resultant stronger aggregation ability than normal single-chain surfactants. Thus, different from the micelle template assembled by CTAB molecules, the aggregates of the $C_{12}C_6C_{12}Br_2$–$HAuCl_4$ complexes are stable enough to be the templates for the gold nanomaterials.

Herein, the spherical aggregates of the $C_{12}C_6C_{12}Br_2$–$HAuCl_4$ complexes are the templates of the spherical gold nanoparticles. The shape of the templates is kept after reduction. As to the gold nanowires, the long fibrillar aggregates of the $C_{12}C_6C_{12}Br_2$–$HAuCl_4$ complexes perform as the templates. With the increase of the $HAuCl_4$ content, the binding of the $AuCl_4^-$ with the headgroups of $C_{12}C_6C_{12}Br_2$ greatly lessens the electrostatic repulsion between the headgroups of the surfactant. Then the $C_{12}C_6C_{12}Br_2$–$HAuCl_4$ complex form worm-like micelles. The worm-like micelles associate into the long fibrillar aggregates. Upon reduction by $NaBH_4$, the gold nanomaterials are generated along the fibrillar aggregates. In order to know the reduction process, TEM was used to monitor the process as shown in Fig. 6. The reaction solution extracted at different reaction time was directly dropped on the TEM grid, and then immersed into liquid nitrogen immediately. Thereafter, the frozen samples were lyophilized for the TEM observation. The image of the gold nanostructures obtained after 30 s reduction clearly shows an assembled line of nanoparticles in one-dimension (Fig. 6a). The arrangement of the nanoparticles oriented in a line strongly implies that the nanoparticles are directed by the fibrillar $C_{12}C_6C_{12}Br_2$–$HAuCl_4$ template. Once the small particles are formed, the particle fusion occurs in succession. The driving force for the fusion is to minimize the surface energy of the system. The image after the duration of 180 s indicates that larger nanoparticles already construct the premature gold nanowires (Fig. 6b). After 24 h intra-particles ripening process (smoothing), the nanowires are formed (Fig. 2d).

Gemini surfactant plays an important role during the period of the particle fusion. The headgroups with two positive charges can efficiently cap on the certain surface of the growing gold nanoparticles, while strong hydrophobic interaction of the surfactant with two chains efficiently pull the particles to be close

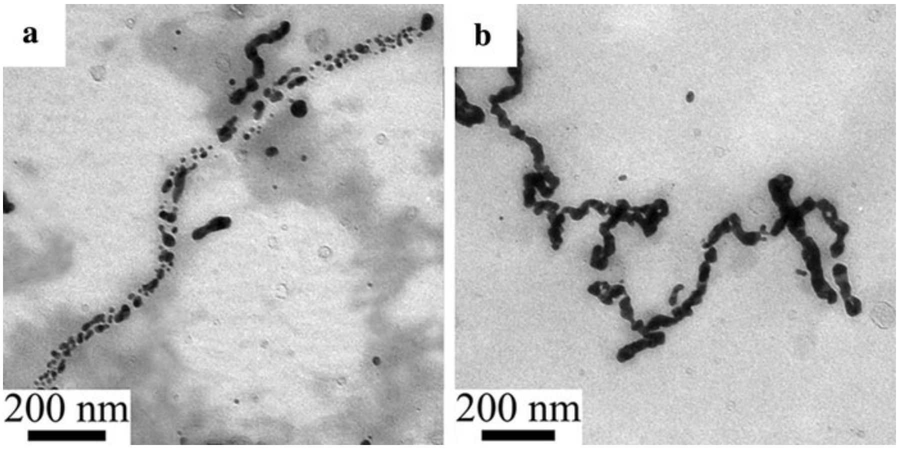

Fig. 6 TEM images of the gold products at $R = 2{:}1$ for the duration of 30 s (**a**) and 180 s (**b**)

enough, facilitating the subsequent fusion process. Previously this enhanced aggregation by strong hydrophobic interaction was also utilized to explain the formation of the nanoparticle superlattice in the presence of gemini surfactant (Bakshi 2009). Moreover, stronger hydrophobic interaction between the gemini surfactants efficiently inhibit the template breakage during the nucleation and growth stages.

As to the braided nanowires, the similar braided nanostructure has not yet been observed in the aggregates of the $C_{12}C_6C_{12}Br_2$–$HAuCl_4$ complexes. The $C_{12}C_6C_{12}Br_2$–$HAuCl_4$ complexes still exist as fibrillar aggregates in the precursor solution where the braided gold nanowires are obtained. Because the fibrillar aggregates contain double layer structure as proved by XRD, the fibrillar aggregates formed at $R = 1{:}1$ and 1:2 are thought to be composed of thinner fibrils. We tried to observe the fine structure of the $C_{12}C_6C_{12}Br_2$–$HAuCl_4$ fibrils by HRTEM, but unfortunately, the fibrils were easily damaged under the irradiation of TEM electron beam (Fig. S2). Therefore, a tentative interpretation on the formation of braided nanowires is suggested as follows. Upon the binding of the $C_{12}C_6C_{12}Br_2$ with more $AuCl_4^-$ anions at $R = 1{:}1$ and 1:2, the $C_{12}C_6C_{12}Br_2$–$HAuCl_4$ complexes self-assembled into thinner fibrils with very low surface charge density. The very low charged fibrils should be more flexible and tend to twist with each others. With the reduction of $NaBH_4$, then the braided nanowires are generated through template-directed aggregation and fusion process of nanoparticles. In brief, the morphologies and the molecular packing modes of the $C_{12}C_6C_{12}Br_2$–$HAuCl_4$ aggregates control the morphologies of the gold nanomaterials. Comparing with conventional single-chain surfactant, the double chains of gemini surfactants promote the aggregation and fusion of the nanoparticles. Therefore, essentially, the presence of the gemini surfactant is the key factor for the formation of the braided nanowires.

Catalytic activities of gold nanomaterials in the $NaBH_4$ reduction of *p*-NA

It is well-known that the catalytic properties of nanomaterials are largely dependent on their size, morphology, specific surface area, and nature of exterior facets, etc. (Min and Friend 2007; Campbell 2004). In general, the nanomaterials with large surface areas and high-index exposed facets display high-catalytic activity, especially for noble-metal nanomaterials (Mostafa et al. 2010; Tian et al. 2007). Here, the gold nanowires, braided gold nanowires and broad braided gold nanowires were selected to be applied to the reduction of *p*-NA with $NaBH_4$. The representative time-dependent UV–Vis absorption spectra and the plot of the absorbance (*A*) at 380 nm versus time are shown for the broad braided nanowires in the Fig. 7a, b. The absorption spectra of the reaction mixture show a gradual decrease for the peak at 380 nm, a progressive development for the peak around 220 nm and the appearance of a new peak at 300 nm (Fig. 7a). ^{1}HNMR result indicates the reduction product is *p*-phenylenediamine with nearly 100 % yield (Fig. S3). The rate constant (*k*) of the catalytic reaction calculated is 16.16×10^{-2} min^{-1} for the broad braided

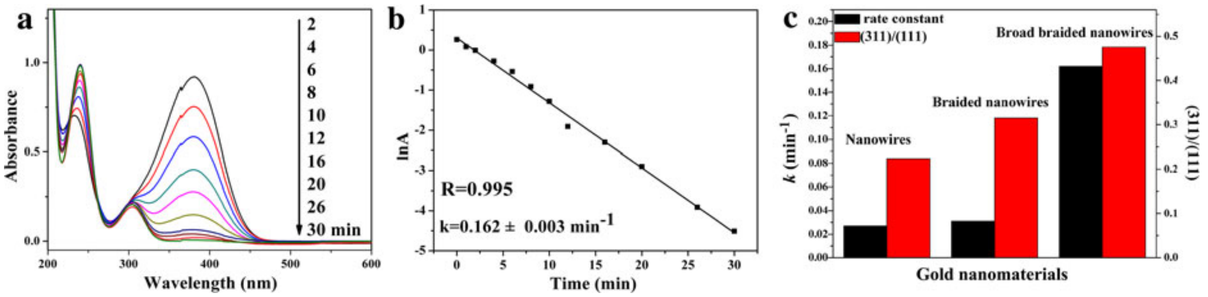

Fig. 7 **a** Successive UV–Vis absorption spectra and **b** the corresponding plot of ln A versus time for the reduction of *p*-NA (0.001 M) with 0.1 M $NaBH_4$ catalyzed by the gold broad braided nanowires. **c** The rate constant (*k*) and the (311)/(111) intensity ratio of the selected gold nanomaterials

nanowires, and 3.11 × 10^{-2} min^{-1} for the braided nanowires, and 2.66 × 10^{-2} min^{-1} for the nanowires. To further understand the catalytic efficiency, the turnover number (TON) and turnover frequency (TOF) were estimated (Kundu et al. 2009; Jia et al. 2012). The TON and TOF values are 4.28 × 10^8, 1.09 × 10^9, and 1.38 × 10^9 mol/mol, and 2.36 × 10^6, 6.98 × 10^6 and 4.58 × 10^7 mol/(mol min) for the nanowires, braided nanowires, and broad braided nanowires, respectively. Obviously, the catalytic activity of the broad braided nanowires is the highest among the three gold nanomaterials. The Brunauer–Emmett–Teller (BET) adsorption analysis showed that the specific surface areas of the nanowires, braided nanowires and broad braided nanowires were 6.22, 6.73, and 11.46 m^2 g^{-1}, respectively, which suggested that the enhanced activities of broad braided nanowires should be partially attributed to the surface areas. Besides, the higher catalytic activity corresponds to the higher (311)/(111) intensity ratio calculated from the XRD data (Fig. 7c). The higher (311)/(111) intensity ratio offers a larger number of atoms of corners and edges (low coordinated atoms), which can also improve the catalytic activity of nanomaterials (Chirea et al. 2011). In addition, the kinks of the braided nanostructures may bring more grain boundaries which may provide additional active sites for catalytic reactions (Qin et al. 2010).

Conclusions

In summary, novel braided gold nanowires were conveniently constructed with a cationic gemini surfactant $C_{12}C_6C_{12}Br_2$. The correlation between the aggregate structures of the $C_{12}C_6C_{12}Br_2$–$HAuCl_4$ complexes and the resultant gold nanomaterials was systematically studied. The results indicate that the complexes of the gemini surfactant $C_{12}C_6C_{12}Br_2$ with $HAuCl_4$ form spherical and fibrillar aggregates, depending on the mole ratio of $C_{12}C_6C_{12}Br_2$ to $HAuCl_4$. The spherical aggregates of the $C_{12}C_6C_{12}Br_2$–$HAuCl_4$ complexes produce spherical gold nanoparticles, while the $C_{12}C_6C_{12}Br_2$–$HAuCl_4$ fibrillar aggregates composed of worm-like aggregates and double layer structures generate gold nanowires and braided nanowires, respectively. The gemini surfactant is a key factor to the formation of the braided nanowires. Fine modulation of the electrostatic interaction between the $C_{12}C_6C_{12}Br_2$ headgroups and $AuCl_4^-$ dictates the transition of the $C_{12}C_6C_{12}Br_2$–$HAuCl_4$ aggregates, which in turn determines the morphology of the final gold products. Especially, the gemini surfactant can form much stable aggregates with $HAuCl_4$, which insures the shape-preserved transformation from templates to gold products. The braided gold nanowires exhibit high-catalytic activity for the reduction of *p*-NA with $NaBH_4$. Moreover, such one-dimensional nanostructures may have distinct electrical and thermal transport properties and mechanical properties and display potential applications in fabricating electronic, optoelctronic, and electrochemical devices (Kuchibhatla et al. 2007; Xia et al. 2003; Murphy et al. 2006; Li et al. 2003; Melosh et al. 2003). This study helps to extend the application of gemini surfactants in material science. Although conventional single-chain surfactants have been widely used in the synthesis of nanomaterials, the utilizations of gemini surfactants are scarce. The gemini surfactant-based template strategy provides a facile route to design various inorganic nanomaterials with novel morphologies and unique applications.

Acknowledgments We are grateful for financial supports from the National Natural Science Foundation of China (21025313, 21021003).

References

Bakshi MS (2009) A simple method of superlattice formation: step-by-step evaluation of crystal growth of gold nanoparticles through seed–growth method. Langmuir 25(21):12697–12705. doi:10.1021/la901767c

Bakshi MS, Possmayer F, Petersen NO (2008) Aqueous-phase room-temperature synthesis of gold nanoribbons: soft template effect of a gemini surfactant. J Phys Chem C 112(22):8259–8265. doi:10.1021/jp801306x

Banerjee IA, Yu L, Matsui H (2003) Location-specific biological functionalization on nanotubes: attachment of proteins at the ends of nanotubes using Au nanocrystal masks. Nano Lett 3(3):283–287. doi:10.1021/nl034038w

Campbell CT (2004) The active site in nanoparticle gold catalysis. Science 306:234–235. doi:10.1126/science.1104246

Chen HM, Hsin CF, Liu RS, Lee JF, Jang LY (2007a) Synthesis and characterization of multi-pod-shaped gold/silver nanostructures. J Phys Chem C 111(16):5909–5914. doi:10.1021/jp070232l

Chen JY, Wiley BJ, Xia YN (2007b) One-dimensional nanostructures of metals: large-scale synthesis and some potential applications. Langmuir 23(8):4120–4129. doi:10.1021/la063193y

Chirea M, Freitas A, Vasile BS, Ghitulica C, Pereira CM, Silva F (2011) Gold nanowire networks: synthesis, characterization, and catalytic activity. Langmuir 27(7):3906–3913. doi:10.1021/la104092b

Cobley CM, Chen JY, Cho EC, Wang LHV, Xia YN (2011) Gold nanostructures: a class of multifunctional materials for biomedical applications. Chem Soc Rev 40:44–56. doi:10.1039/B821763G

Daniel MC, Astruc D (2004) Gold nanoparticles: assembly, supramolecular chemistry, quantum-size-related properties, and applications toward biology, catalysis, and nanotechnology. Chem Rev 104(1):293–346. doi:10.1021/cr030698+

Deng ML, Yu DF, Hou YB, Wang YL (2009) Self-assembly of peptide – amphiphile C12–Aβ(11–17) into nanofibrils. J Phys Chem B 113(25):8539–8544. doi:10.1021/jp904289y

Esumi K, Hara J, Aihara N, Usui K, Torigoe K (1998) Preparation of anisotropic gold particles using a gemini surfactant template. J Colloid Interface Sci 208(2):578–581. doi:10.1006/jcis.1998.5852

Fan YX, Hou YB, Xiang JF, Yu DF, Wu CX, Tian MZ, Han YC, Wang YL (2011) Synthesis and aggregation behavior of a hexameric quaternary ammonium surfactant. Langmuir 27(17):10570–10579. doi:10.1021/la202453c

Groth C, Nydén M, Holmberg K, Kanicky JR, Shah DO (2004) Kinetics of the self-assembly of gemini surfactants. J Surfactants Deterg 7(3):247–255. doi:10.1007/s11743-004-0308-8

Habas SE, Lee H, Radmilovic V, Somorjai GA, Yang PD (2007) Shaping binary metal nanocrystals through epitaxial seeded growth. Nat Mater 6:692–697. doi:10.1038/nmat1957

Han YC, Wang YL (2011) Aggregation behavior of gemini surfactants and their interaction with macromolecules in aqueous solution. Phys Chem Chem Phys 13:1939–1956. doi:10.1039/C0CP01196G

Han W, Yi LX, Zhao N, Tang AW, Gao MY, Tang ZY (2008) Synthesis and shape-tailoring of copper sulfide/indium sulfide-based nanocrystals. J Am Chem Soc 130(39):13152–13161. doi:10.1021/ja8046393

Holmberg K (2004) Surfactant-templated nanomaterials synthesis. J Colloid Interface Sci 274(2):355–364. doi:10.1016/j.jcis.2004.04.006

Hou YB, Han YC, Deng ML, Xiang JF, Wang YL (2010) Aggregation behavior of a tetrameric cationic surfactant in aqueous solution. Langmuir 26(1):28–33. doi:10.1021/la903672r

Huang X, Cao MW, Wang JB, Wang YL (2006) Controllable organization of a carboxylic acid type gemini surfactant at different pH values by adding copper (II) Ions. J Phys Chem B 110(39):19479–19486. doi:10.1021/jp0630121

Huang XH, Neretina S, El-Sayed MA (2009) Gold nanorods: from synthesis and properties to biological and biomedical applications. Adv Mater 21(48):4880–4910. doi:10.1002/adma.200802789

Jana NR (2005) Gram-scale synthesis of soluble, near-monodisperse gold nanorods and other anisotropic nanoparticles. Small 1(8–9):875–882. doi:10.1002/smll.200500014

Jeong GH, Kim M, Lee YW, Choi W, Oh WT, Park QH, Han SW (2009) Polyhedral Au nanocrystals exclusively bound by 110 facets: the rhombic dodecahedron. J Am Chem Soc 131(5):1672–1673. doi:10.1021/ja809112n

Jia H, Gao X, Chen Z, Liu G, Zhang X, Yan H, Zhou H, Zheng L (2012) The high yield synthesis and characterization of gold nanoparticles with superior stability and their catalytic activity. CrystEngComm 14:7600–7606. doi:10.1039/C2CE25840D

Kijima T, Yoshimura T, Uota M, Ikeda T, Fujikawa D, Mouri S, Uoyama S (2004) Noble-metal nanotubes (Pt, Pd, Ag) from lyotropic mixed-surfactant liquid-crystal templates. Angew Chem Int Ed 43(2):228–232. doi:10.1002/anie.200352630

Kim F, Sohn K, Wu J, Huang J (2008) Chemical synthesis of gold nanowires in acidic solutions. J Am Chem Soc 130(44):14442–14443. doi:10.1021/ja806759v

Kuchibhatla SVNT, Karakoti AS, Bera D, Seal S (2007) One dimensional nanostructured materials. Prog Mater Sci 52:699–913. doi:10.1016/j.pmatsci.2006.08.001

Kundu S, Lau S, Liang H (2009) Shape-controlled catalysis by cetyltrimethylammonium bromide terminated gold nanospheres, nanorods, and nanoprisms. J Phys Chem C 113(13):5150–5156. doi:10.1021/jp811331z

Li X, Gao H, Murphy CJ, Caswell KK (2003) Nanoindentation of silver nanowires. Nano Lett 3(11):1495–1498. doi:10.1021/nl034525b

Li LS, Wang ZJ, Huang T, Xie JL, Qi LM (2010) Porous gold nanobelts templated by metal–surfactant complex nanobelts. Langmuir 26(14):12330–12335. doi:10.1021/la1015737

Lin HP, Mou CY (2002) Structural and morphological control of cationic surfactant-templated mesoporous silica. Acc Chem Res 35(11):927–935. doi:10.1021/ar000074f

Lu XM, Yavuz MS, Tuan HY, Korgel BA, Xia YN (2008) Ultrathin gold nanowires can be obtained by reducing polymeric strands of oleylamine–AuCl complexes formed via aurophilic interaction. J Am Chem Soc 130(28): 8900–8901. doi:10.1021/ja803343m

Melosh NA, Boukai A, Diana F, Gerardot B, Badolato A, Petroff PM, Heath JR (2003) Ultra high density nanowire lattices and circuits. Science 300:112–115. doi:10.1126/science.1081940

Menger FM, Keiper JS (2000) Gemini surfactants. Angew Chem Int Ed 39(11):1906–1920. doi:10.1002/1521-3773(20000602)39:11<1906:AID-ANIE1906>3.0.CO;2-Q

Millstone JE, Hurst SJ, Métraux GS, Cutler JI, Mirkin CA (2009) Colloidal gold and silver triangular nanoprisms. Small 5(6):646–664. doi:10.1002/smll.200801480

Min BK, Friend CM (2007) Heterogeneous gold-based catalysis for green chemistry: low-temperature CO oxidation and propene oxidation. Chem Rev 107(6):2709–2724. doi:10.1021/cr050954d

Mostafa S, Behafarid F, Croy JR, Ono LK, Li L, Yang JC, Frenkel AI, Cuenya BR (2010) Shape-dependent catalytic properties of Pt nanoparticles. J Am Chem Soc 132(44): 15714–15719. doi:10.1021/ja106679z

Murphy CJ, Gole AM, Hunyadi SE, Orendorff CJ (2006) One-dimensional colloidal gold and silver nanostructures. Inorg Chem 45(19):7544–7554. doi:10.1021/ic0519382

Murphy CJ, Thompson LB, Chernak DJ, Yang JA, Sivapalan ST, Boulos SP, Huang JY, Alkilany AM, Sisco PN (2011) Gold nanorod crystal growth: from seed-mediated synthesis to nanoscale sculpting. Curr Opin Colloid Interface Sci 16(2):128–134. doi:10.1016/j.cocis.2011.01.001

Nikoobakht B, El-Sayed MA (2003) Preparation and growth mechanism of gold nanorods (NRs) using seed-mediated growth method. Chem Mater 15(10):1957–1962. doi:10.1021/cm020732l

Pérez-Juste J, Pastoriza-Santos I, Liz-Marzán LM, Mulvaney P (2005) Gold nanorods: synthesis, characterization and applications. Coord Chem Rev 249(17–18):1870–1901. doi:10.1016/j.ccr.2005.01.030

Pileni MP (2003) The role of soft colloidal templates in controlling the size and shape of inorganic nanocrystals. Nat Mater 2:145–150. doi:10.1038/nmat817

Qiao Y, Wang YJ, Yang ZY, Lin YY, Huang JB (2011) Self-templating of metal-driven supramolecular self-assembly: a general approach toward 1D inorganic nanotubes. Chem Mater 23(5):1182–1187. doi:10.1021/cm102649y

Qin GW, Pei WL, Ma XM, Xu XN, Ren YP, Sun W, Zuo L (2010) Enhanced catalytic activity of Pt nanomaterials: from monodisperse nanoparticles to self-organized nanoparticle-linked nanowires. J Phys Chem C 114(15):6909–6913. doi:10.1021/jp910864w

Sau TK, Murphy CJ (2004) Room temperature, high-yield synthesis of multiple shapes of gold nanoparticles in aqueous solution. J Am Chem Soc 126(28):8648–8649. doi:10.1021/ja047846d

Sharma V, Park K, Srinivasarao M (2009) Colloidal dispersion of gold nanorods: historical background, optical properties, seed-mediated synthesis, shape separation and self-assembly. Mater Sci Eng R 65(1–3):1–38. doi:10.1016/j.mser.2009.02.002

Skrabalak SE, Chen JY, Sun YG, Lu XM, Au L, Cobley CM, Xia YN (2008) Gold nanocages: synthesis, properties, and applications. Acc Chem Res 41(12):1587–1595. doi:10.1021/ar800018v

Tian N, Zhou ZY, Sun SG, Ding Y, Wang ZL (2007) Synthesis of tetrahexahedral platinum nanocrystals with high-index facets and high electro-oxidation activity. Science 316:732–735. doi:10.1038/nchina.2007.89

Ulbricht W, Zana R (2001) Alkanediyl-α, ω-bis(dimethylalkylammonium bromide) surfactants: part 8. Pressure-jump study of the kinetics of micellar equilibria in aqueous solutions of alkanediyl- α, ω -bis(dimethyldodecylammonium bromide) surfactants. Colloids Surf A 183–185:487–494. doi:10.1016/S0927-7757(01)00560-X

Vazquez-Mena O, Villanueva G, Savu V, Sidler K, van den Boogaart MAF, Brugger J (2008) Metallic nanowires by full wafer stencil lithography. Nano Lett 8(11):3675–3682. doi:10.1021/nl801778t

Wan Y, Zhao DY (2007) On the controllable soft-templating approach to mesoporous silicates. Chem Rev 107(7):2821–2860. doi:10.1021/cr068020s

Wang Y, Wang QX, Sun H, Zhang WQ, Chen G, Wang YW, Shen XS, Han Y, Lu XM, Chen HY (2011) Chiral transformation: from single nanowire to double helix. J Am Chem Soc 133(50):20060–20063. doi:10.1021/ja208121c

Wu CX, Hou YB, Deng ML, Huang X, Yu DF, Xiang JF, Liu Y, Li ZB, Wang YL (2010) Molecular conformation-controlled vesicle/micelle transition of cationic trimeric surfactants in aqueous solution. Langmuir 26(11):7922–7927. doi:10.1021/la9048067

Xia Y, Yang P, Sun Y, Wu Y, Mayers B, Gates B, Yin Y, Kim F, Yan H (2003) One-dimensional nanostructures: synthesis, characterization, and applications. Adv Mater 15(5): 353–389. doi:10.1002/adma.200390087

Xiao JY, Qi LM (2011) Surfactant-assisted, shape-controlled synthesis of gold nanocrystals. Nanoscale 3:1383–1396. doi:10.1039/c0nr00814a

Yi LX, Gao MY (2011) From ultrathin two-dimensional djurleite nanosheets to one-dimensional nanorods comprised of djurleite nanoplates: synthesis, characterization, and formation mechanism. Cryst Growth Des 11(4):1109–1116. doi:10.1021/cg101322s

Zana R, Benrraou M, Rueff R (1991) Alkanediyl-alpha, omega-bis(dimethylalkylammonium bromide) surfactants. 1. Effect of the spacer chain length on the critical micelle concentration and micelle ionization degree. Langmuir 7(6):1072–1075. doi:10.1021/la00054a008

Zhang J, Du J, Han B, Liu Z, Jiang T, Zhang Z (2006) Sonochemical formation of single-crystalline gold nanobelts. Angew Chem Int Ed 45(7):1116–1119. doi:10.1002/anie.200503762